 doi:10.20944/preprints202008.0666.v1

Article

Fabrication of Alumina Doped Optical Fiber Preforms by MCVD-Metal Chelate Doping Method

K.A. Mat Sharif [2], Nasr Y.M. Omar [1], M.I. Zulkifli [2], S.Z. Muhamad Yassin [2], and H.A. Abdul-Rashid [1,*]

[1] Fiber Optics Research Center, Faculty of Engineering, Multimedia University, Cyberjaya, Malaysia; nasr-omar@hotmail.com
[2] Telekom Malaysia Research & Development Sdn. Bhd., Malaysia; khairulmcvd@gmail.com (K.S.); mohdimran@tmrnd.com.my (M.Z.); shahrinzen@tmrnd.com.my (S.Y.)
* Correspondence: hairul@mmu.edu.my

Potential Application: Fabrication of rare-earth doped fiber amplifiers and high-power fiber lasers.

Abstract: This paper reports on the fabrication of alumina doped preforms using MCVD-vapor phase chelate delivery system with $Al(acac)_3$ as the precursor. The objectives of the work are to study the deposition process, the efficiency of the fabrication process, and the quality of the fabricated fiber preforms. Two parameters are studied, $Al(acac)_3$ sublimator temperature (T_{Al}°C) and deposition direction (i.e. downstream and upstream). Other parameters such as oxygen flow and deposition temperature are fixed. The results showed that a high uniformity of refractive index difference (%RSD < 2%) and core size (%RSD < 2.4%) was obtained along the preform length using downstream deposition while for the combined upstream and downstream deposition the uniformity was deteriorated. The process efficiency was found to be about 21% for T_{Al}°C of 185°C and downstream deposition. From the EDX elemental analysis, the refractive index was found to increase by 0.0025 per mole percent of alumina.

Keywords: MCVD; chelate delivery system; $Al(acac)_3$; alumina; vapor phase doping; EDX

1. Introduction

Alumina (Al_2O_3) is an interesting dopant material for silica optical fiber technology. It does not only function as an index raiser but also helps dissolve other co-dopants such as rare-earth elements in the silica matrix. Thus, alumina is very essential to the fabrication of rare-earth doped fiber amplifiers and high-power fiber lasers. The use of alumina was first reported by Maurer and Schultz [1] in 1972 for passive fiber applications followed by Simpson and Macchesney [2], Ohmori et al. [3], Roba [4], Wang et al. [5,6] and Čampelj et al. [7]. The fabrication techniques used were outside vapor deposition (OVD), vertical axial deposition (VAD), and modified chemical vapor deposition (MCVD). With the rapid progress on rare-earth specialty fibers, more research is being focused on incorporating alumina in silica particularly by the MCVD method. The most common technique for doping alumina is the conventional MCVD with solution doping (non-vapor phase) (e.g., [8]). This technique has been very successful in the fabrication of fiber amplifiers such as erbium doped fiber (EDF). However, the technique suffers from limitations including the inability to deliver advanced fiber design requirements such as high dopant concentration, large core and precise wave guiding structure. Furthermore, due to the nature of the MCVD solution doping process that involves several stages, it tends to degrade the quality of the preform or fiber.

Another alternative technique is the MCVD with chelate delivery system which was first reported by Tumminelli et al. [9]. This technique offers in-situ vapor phase deposition of dopants in

Preprints (www.preprints.org) | NOT PEER-REVIEWED | Posted: 30 August 2020 doi:10.20944/preprints202008.0666.v1

a controllable process thus improving the quality of the fabricated preform or fiber. Since the study by Tumminelli et al., several research groups have reported on the use of MCVD with chelate delivery system [e.g., 10–16]. In most of these studies, anhydrous aluminum chloride ($AlCl_3$) has been used as the precursor for alumina. $AlCl_3$ is commonly used due to its relatively high vapor pressure. In this paper, we report on the fabrication of alumina doped preforms using aluminum acetylacetonate ($Al(C_5H_7O_2)_3$; $Al(acac)_3$). Even though $Al(acac)_3$ has lower vapor pressure than $AlCl_3$, it exhibits some advantages over $AlCl_3$ including its low cost, non-corrosive properties, and chemical stability. However, the conversion of $Al(acac)_3$ to Al_2O_3 requires more oxygen (compared to $AlCl_3$) in order to eliminate incomplete oxidation of $Al(acac)_3$ which can lead to carbon contamination. The total gas flow rate (oxygen and carrier gas) Q_T is thus considerably higher compared to standard MCVD process. This entails the study of the chemistry and the deposition mechanism involved as well as the effect of various process parameters on the deposition and incorporation efficiency of the Al_2O_3 particles formed during the process. In this work, we studied the fabrication process of alumina doped silica fiber preforms with different $Al(acac)_3$ sublimator temperature, (T_{Al}°C) and deposition direction (i.e. downstream and upstream). Other parameters such as total oxygen flow, deposition temperature, carriage speed (V_b), and spindle rotation were fixed. The fabricated preforms were checked for radial and longitudinal uniformity. The efficiency of the fabrication process was also determined by comparing the Al_2O_3 concentration obtained from energy dispersive X-ray spectroscopy (EDX) analyses with that derived theoretically.

Our chelate delivery system is depicted in Figure 1. The $Al(acac)_3$ is placed in a sublimator (maximum operating temperature of 220°C) and the vapor is carried to the reaction zone by a constant flow of high purity helium gas using heated stainless-steel tubes. A ceramic heater is placed at the end of the delivery tube and just before the MCVD main oxyhydrogen burner in order to prevent any condensation of $Al(acac)_3$ vapor on the walls of the glass substrate tube. The refractive index profile and longitudinal uniformity of the fabricated preforms were determined using a preform analyzer (*Photon Kinetics*, P104). The fabricated preforms were pulled into fibers (125µm in diameter) using a standard fiber drawing tower and were subjected to an elemental quantitative analysis using EDX spectroscopy. The EDX analyses were performed using the point identification technique with 10 × 10 grid points and an acquisition time of 240 s per point.

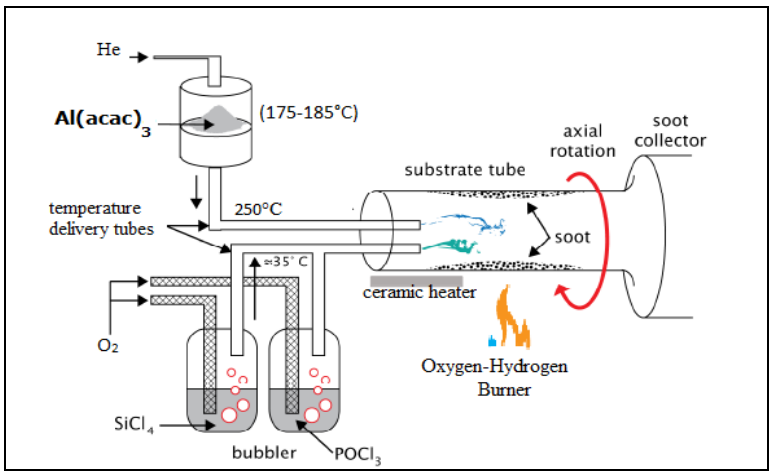

Figure 1. A schematic diagram for the MCVD-chelate delivery system [14]. The $Al(acac)_3$ is placed in a sublimator consisting of a stainless-steel plate, a heater and a gas system (outlet and inlet). The stainless-steel delivery tube is equipped with a heater to prevent any $Al(acac)_3$ vapor condensation. The standard MCVD delivery lines and the chelate delivery line are joined with special rotary seal. A ceramic heater is placed just before the hot zone.

2. Materials and Methods

The fabrication process is divided into two major steps; first is the MCVD process and second is the $Al(acac)_3$ oxidation process. These steps are then followed by a standard MCVD procedure

Preprints (www.preprints.org) | NOT PEER-REVIEWED | Posted: 30 August 2020 doi:10.20944/preprints202008.0666.v1

including sintering and collapsing of the glass substrate tube to a solid preform. At the MCVD step, the glass substrate tube (25 (OD) × 19 (ID) mm) is first etched with SF_6 for several passes of the oxyhydrogen burner at very high temperature. Several layers of SiO_2 are then deposited and sintered to act as a barrier between the glass substrate tube and the preform's core. Finally, for the preform's core, two layers of unsintered SiO_2 are deposited. For the $Al(acac)_3$ oxidation step, $Al(acac)_3$ vapor is delivered to the glass substrate tube where it is converted to Al_2O_3 at high temperature and in the presence of high purity oxygen gas. Table 1 lists the process parameters used in this work. For preform 1 (P1), $Al(acac)_3$ is sublimed at T_{Al}°C of 175°C, with carrier gas (He) and O_2 flow rates of 1440 and 2400 sccm, respectively. The deposition temperature (T_{dep}°C) is fixed at 1850°C with carriage speed (V_{dep}) of 100 mm/min and spindle rotation of 50 rpm (rotation per minute). A total of 10 layers are deposited in the downstream direction. For preforms 2 (P2) and 3 (P3), T_{Al}°C is fixed at 185°C with P2 having a total of 8 layers deposited in the downstream direction and P3 having 7 layers deposited in each direction (i.e. downstream and upstream). Figure 2 illustrates the downstream and upstream deposition directions.

Table 1. Process parameters and calculated flow rates for the fabrication process

Preform	T_{Al} (°C)	Gas Flow (sccm)		Q_v (g/min)[1]	Q_m (g/min)[1]	Number of passes		Total Q_m (g)[1]
		He	O_2			Forward	Backward	
P1	175	1440	2400	0.062	0.97×10^{-2}	10	-	0.34
P2	185			0.116	1.82×10^{-2}	8	-	0.58
P3						7	7	1.02

[1] V_{dep} 100 mm/min, Q_v is the flow rate of reactant (g/min), Q_m is the product's flow rate (g/min) and total Q_m is the total amount of product during process (g). The vapor pressure for $Al(acac)_3$ is taken from [17].

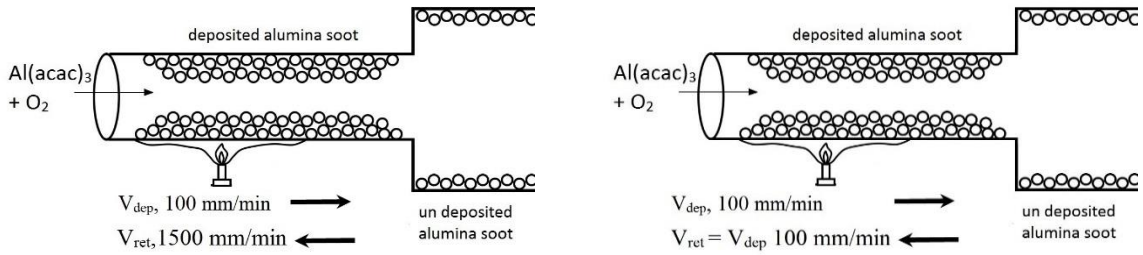

(**a**) (**b**)

Figure 2. (**a**) downstream deposition direction with V_{dep} 100 mm/min and V_{ret} (burner return speed) 1500 mm/min; and (**b**) downstream and upstream deposition directions (V_{dep} 100 mm/min and V_{ret} = V_{dep} = 100 mm/min).

The refractive index profiles (RIPs) of the fabricated preforms are obtained using a preform analyzer (*Photon Kinetics*, P104). The longitudinal uniformity of the fabricated preforms is determined by scanning the preform in 2.0 cm intervals. For each preform, an approximately 3.0 mm thick disk (with known index difference) is cut of the preform, polished and subjected to EDX point identification analyses (10 × 10 grid points are mapped in each preform's core area). The fibers drawn from the fabricated preforms are also subjected to EDX point identification analyses in order to determine the amount and radial distribution of alumina in the core region. The efficiency of the fabrication process is determined by dividing the alumina concentration obtained from EDX analyses by that derived theoretically.

3. Results and Discussion

Figure 3 shows the oxidation process of $Al(acac)_3$ at T_{dep} 1850°C and oxygen flow rate of 2400 sccm. As the $Al(acac)_3$ vapor passes through the hot zone, alumina particles (soot) are formed and

Preprints (www.preprints.org) | NOT PEER-REVIEWED | Posted: 30 August 2020 doi:10.20944/preprints202008.0666.v1

then deposited on the substrate tube wall downstream of the oxyhydrogen burner due to thermophoretic forces. It is observed that the alumina soot is deposited further from the oxyhydrogen burner (i.e. longer taper region). This can be attributed to the high total gas flow rate (Q_T) used during the oxidation process (3840 sccm). The length over which the deposition takes place is proportional to Q_T/α [18] where α is the thermal diffusivity. Since the hot zone created by our oxyhydrogen burner is small (~2 cm in length), and Q_T is high, the residence time of $Al(acac)_3$ inside the hot zone is short. This results in the formation of predominantly fine alumina particles that can be uniformly distributed along the substrate tube. Continuous movement of the hot zone results in fusion of the deposited alumina particles and incorporation into the silica soot. The deposited alumina/silica layers are then vitrified (in oxygen atmosphere) into transparent glassy material.

Figure 3. $Al(acac)_3$ oxidation process with MCVD, where the fine white particles (or alumina soot) are deposited along the glass substrate tube while the $Al(acac)_3$ vapor passes through the hot zone. The figure also shows the ceramic heater used to prevent the condensation of $Al(acac)_3$ vapor prior to reaching the hot zone.

Figures 4(a) and (b) show the refractive index profiles for P1 (T_{Al} 175°C) and P2 (T_{Al} 185°C), respectively. Figures 4(c) and (d) display the longitudinal uniformity of P1 (average $\Delta n = 0.0036$) and P2 (average $\Delta n = 0.0124$), respectively. As can be seen from the figure, P1 and P2 show good longitudinal uniformity with a slight variation in the refractive index difference (%RSD 1% and 2%, respectively). This good longitudinal uniformity can be ascribed to the high total gas flow rate (Q_T) used; and short hot zone and residence time which result in the production of fine and uniform alumina particles as discussed above. As is illustrated in Figures 5 (a)-(d), the core (d_{core}) and preform ($d_{preform}$) diameters for P1 are 1.2 mm (%RSD 2.4%) and 15.0 mm (%RSD 1.2%), respectively, whereas those for P2 are 1.44 mm (%RSD 1.4%) and 15.4 mm (%RSD 1.0%), respectively. This shows that it is possible to fabricate alumina doped silica preforms with high uniformity of Δn and core size using $Al(acac)_3$ and chelate vapor delivery system.

For preform P3, the deposition of alumina is performed in both the downstream and upstream directions. The upstream deposition mode is normally used to utilize higher temperature without sintering the produced soot [19, 20]. In P3, it is observed that the downstream deposition shows the same behavior as P2. In the upstream deposition, however, more alumina with large particle size distribution is produced. In this case, the alumina particles are deposited behind the moving burner and are partially sintered since the burner is moving away towards the reactants inlet. In addition, the upstream deposition mode provides higher temperature and longer hot zone which in turn result in longer residence time and enhanced conversion or oxidation of $Al(acac)_3$. This would cause more particle nucleation and agglomeration; and hence larger particle size distribution in the produced alumina soot [19]. In both P2 and P3, the effect of Q_T/α is the same where the length of deposition is observed to be long (i.e. taper region). It is worth mentioning that during the sintering

Preprints (www.preprints.org) | NOT PEER-REVIEWED | Posted: 30 August 2020 doi:10.20944/preprints202008.0666.v1

process for P3 a red glow with an intensity increasing towards the exhaust tube is observed along the substrate tube (Figure 6(a)). This is indicative of the high concentration of alumina and is manifest in the collapsed preform where the core has an opaque center stretching from about the middle of the preform to the outlet with an increasing opacity towards the outlet (Figure 6(b)). This may be attributed to the deposition of Al_2O_3 in the tiny spaces between silica soot particles. The high temperatures encountered during sintering and collapse may then be enough to cause some aluminum diffusion into silica and therefore producing regions of alumina-rich silicates. The slow cooling of the produced materials as the burner moves away from these regions promotes solidification to a crystalline (rather than an amorphous) phase causing opacity of the core. Another explanation is the formation of alumina-rich silicates by phase separation and crystallization. This may take place when the binary oxide mixture (Al_2O_3/SiO_2) encounters a suitable temperature during sintering or collapse provided that the aluminum concentration is high enough [21].

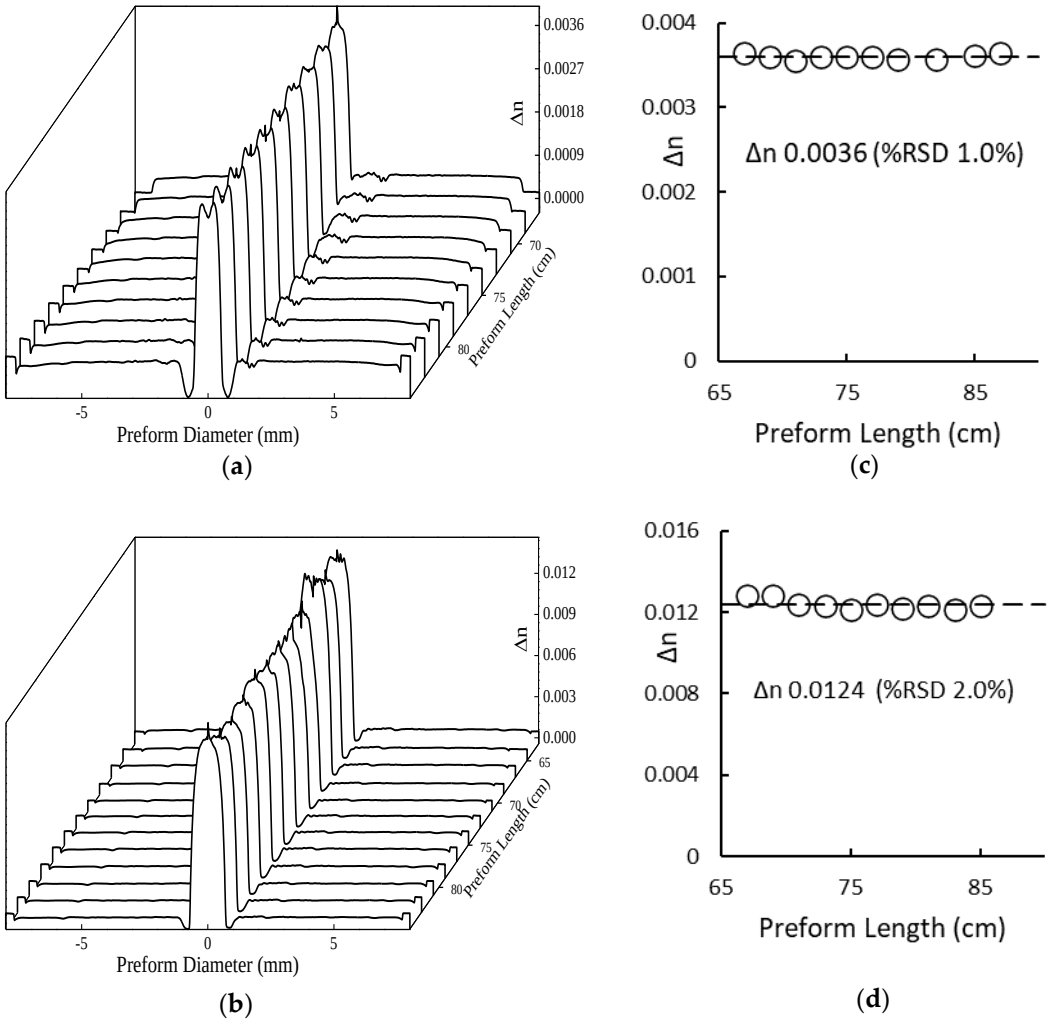

Figure 4. (**a**) and (**b**) show the refractive index profiles for P1 and P2 along the preform length; (**c**) and (**d**) illustrate the longitudinal variation in the refractive index difference (Δn) for P1 and P2, respectively.

Preprints (www.preprints.org) | NOT PEER-REVIEWED | Posted: 30 August 2020 doi:10.20944/preprints202008.0666.v1

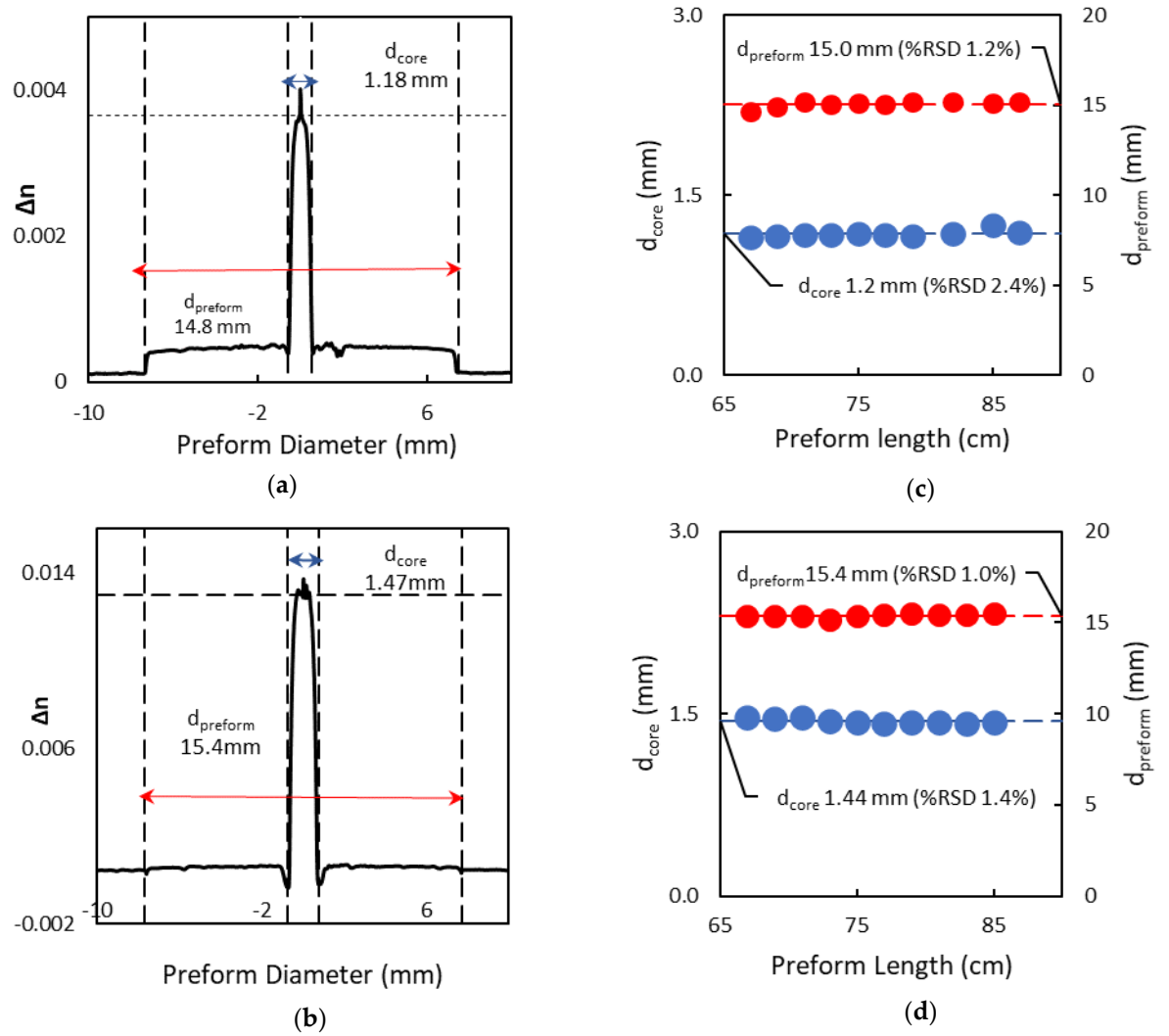

Figure 5. (**a**) and (**b**) refractive index profiles for P1 and P2, respectively, obtained at the inlet position and showing the measurements for $d_{preform}$ and d_{core}; (**c**) and (**d**) longitudinal uniformity of $d_{preform}$ and d_{core} for P1 and P2, respectively.

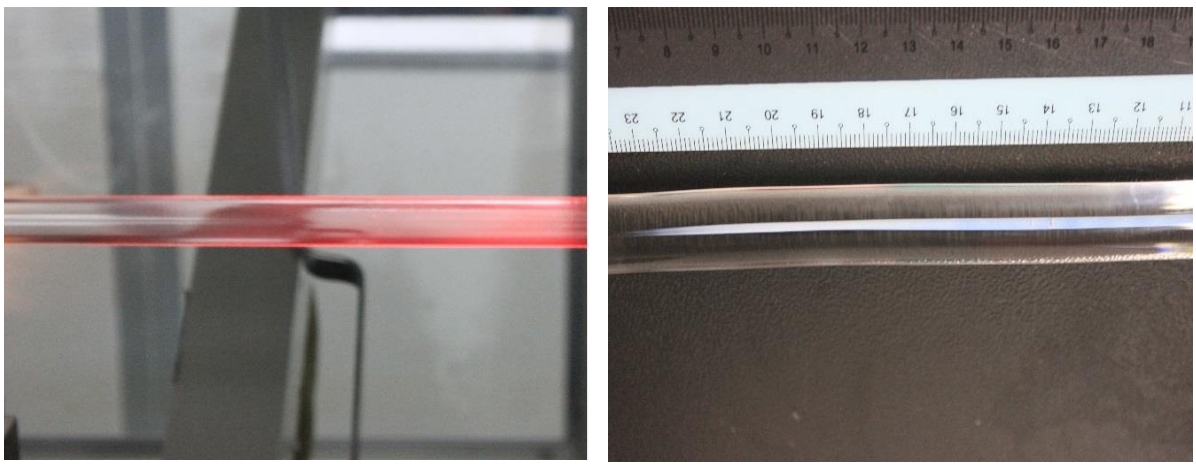

(**a**) (**b**)

Figure 6. (**a**) P3 sintering process with oxygen flow rate of 1000 sccm, temperature of 2000-2100°C, and V_b of 125 mm/min. The red glow is an indicator of the high alumina content in the preform. (**b**) shows the opaque regions in the core due to the presence of Al-rich aluminosilicate crystallites.

Preprints (www.preprints.org) | NOT PEER-REVIEWED | Posted: 30 August 2020 doi:10.20944/preprints202008.0666.v1

It should be pointed out that even though the upstream deposition yielded more alumina, the uniformity in the longitudinal refractive index difference was significantly deteriorated. However, the uniformity could be improved with cooling mechanism as reported by Bubnov et al. [22]. Figure 7(a) illustrates the refractive index profile for P3. The variation in the longitudinal refractive index difference is rather small along the first 13 cm from the inlet (%RSD 4%, Figure 7(b)). It is, however, significantly high along the full length of the preform. The highest core-to-cladding refractive index difference is found to be 0.027 and is for the region of the preform adjacent to the outlet. It is noticed that the opacity in the core is pronounced when the core-to-cladding refractive index difference is greater than 0.015 (~ 6 mol% Al_2O_3). This is consistent with the conclusion that the opaque regions in the core of the preform are attributable to the formation of Al-rich aluminosilicate crystalline phase. One possible aluminosilicate crystalline phase is mullite ($3Al_2O_3.2SiO_2$). X-ray diffraction and Raman spectroscopy analyses carried out by Abramov et al. [23] have indicated that high temperature annealing of aluminosilicate fibers and preforms gives rise to the formation of crystalline mullite phase. It should be mentioned that rapid cooling rate may prevent crystallization in the core of the preform although such rate is typically much higher than that achieved during the MCVD process.

The energy dispersive X-ray spectroscopy (EDX) method is used to investigate the Al distribution and content across the core of the preforms and fibers. The EDX point identification analyses are carried out to support and complement the afore-discussed refractive index profile results. The EDX results for preform P3 are illustrated in Figures 8(a) and (b). As can be seen from Figure 8(a), the Al distribution across the core region is uniform and matches the RIP where the Al content gradually increases, reaches a maximum and then gradually decreases. The Al concentration is highest in the center of the core and is found to range from 8.6 to 9.9 wt.%.

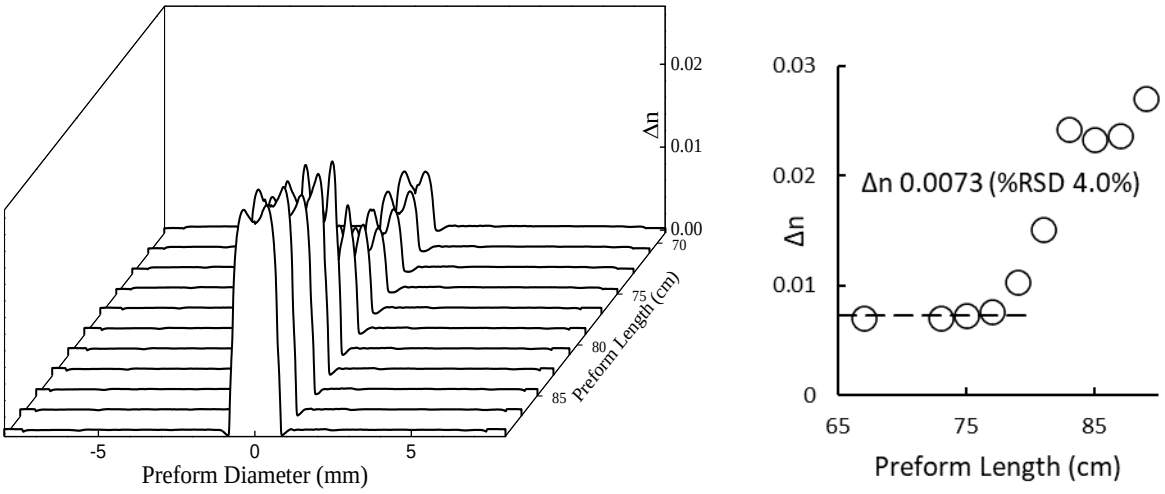

Figure 7. (**a**) Shows the refractive index profile and (**b**) the longitudinal variation in the refractive index difference (Δn) for preform P3.

Preprints (www.preprints.org) | NOT PEER-REVIEWED | Posted: 30 August 2020 doi:10.20944/preprints202008.0666.v1

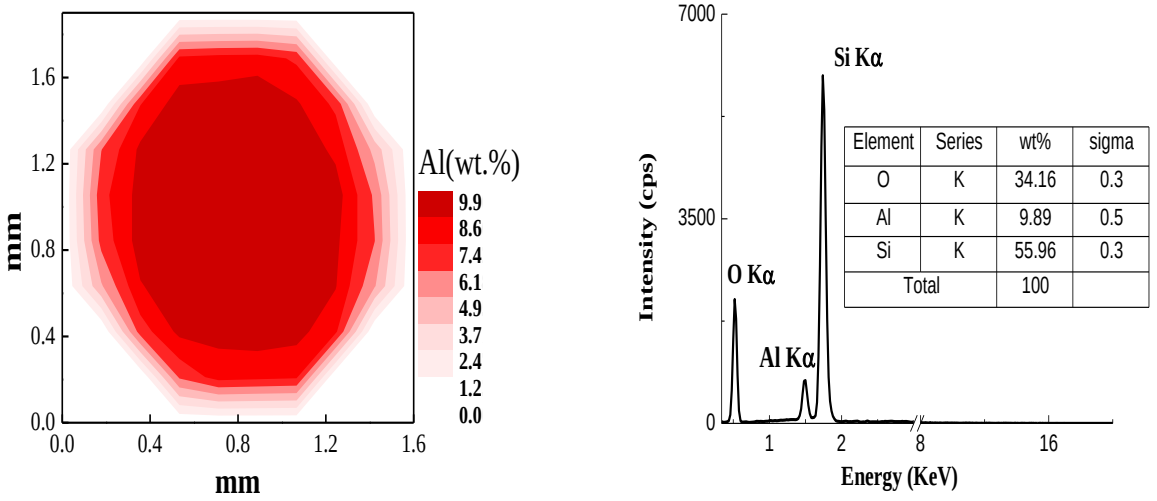

(**a**) (**b**)

Figure 8. (**a**) contour plot of Al concentration in the core region of preform P3. The EDX point identification measurements are performed for 10 × 10 grid points covering an area of 2.0 × 2.0 mm. The sample for EDX analysis is cut of the edge of the preform adjacent to the outlet. (**b**) EDX spectrum measured at the point with the highest Al concentration (9.9 wt.%). The inset table lists the wt.% of Al, Si and O.

Figures 9(a)-(c) show contour plots of Al distribution for fibers F1, F2, and F3, respectively that are drawn from preforms P1, P2 and P3, respectively. In general, the Al distribution for all fibers shows the same pattern with the highest Al content being located at the center of the core area. The maximum Al concentration for fibers F1, F2 and F3 is 1.7, 4.3 and 3.2 wt.%, respectively. This corresponds to an alumina concentration of 1.9, 4.9 and 3.7 mole% for F1, F2 and F3, respectively. In the current study, the fabrication process efficiency is measured by dividing the alumina content obtained from EDX analyses of fibers by that derived theoretically. For the fabricated fibers F1 and F2, the process efficiency is found to be 11 and 21%, respectively. These values indicate that the T_{Al}°C is a critical factor; an increase in T_{Al}°C of 10°C resulted in 3.3 times increase in Al_2O_3 content. The relationship between Δn (obtained from RIP) and Al_2O_3 mol% (obtained from EDX analysis) is plotted in Figure 10. As can be observed from the figure, the refractive index of silica increases by 0.0025 per mol% of Al_2O_3. This is in line with the results obtained by Bubnov et al. [24] where the authors used MCVD vapor phase technique with $AlCl_3$ as the precursor.

Preprints (www.preprints.org) | NOT PEER-REVIEWED | Posted: 30 August 2020 doi:10.20944/preprints202008.0666.v1

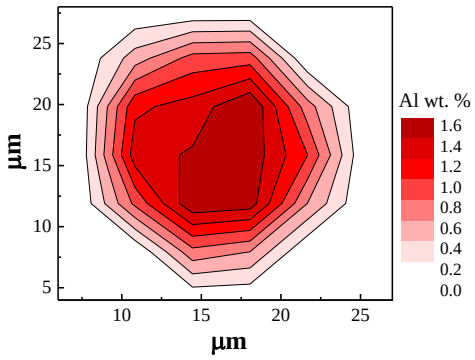

(**a**)

	wt.%	σ wt.%	mole%	
Si	45.28	0.4	SiO_2	98.1
O	53.06	0.3		
Al	1.66	0.09	Al_2O_3	1.9

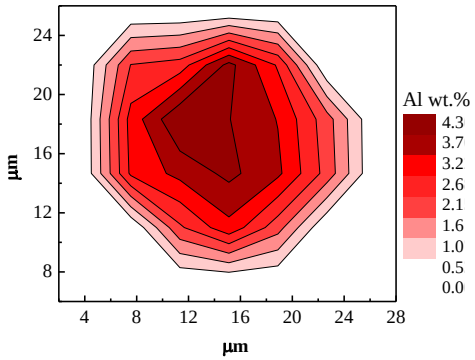

(**b**)

	wt.%	σ wt.%	mole%	
Si	42.95	0.5	SiO_2	95.1
O	52.75	0.3		
Al	4.30	0.1	Al_2O_3	4.9

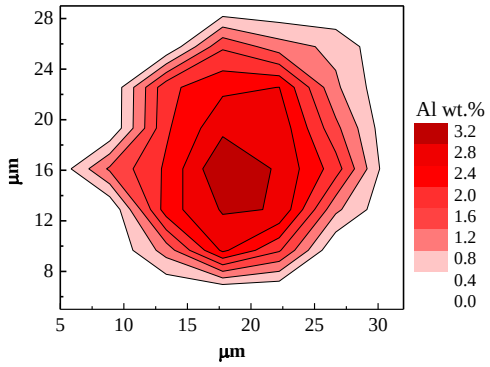

(**c**)

	wt.%	σ wt.%	mole%	
Si	43.9	0.5	SiO_2	96.3
O	52.8	0.4		
Al	3.22	0.1	Al_2O_3	3.7

Figure 9. Contour plots of Al distribution across the core of fibers (**a**) F1, (**b**) F2 and (**c**) F3. The highest Al concentration detected in F1, F2 and F3 is 1.7, 4.3 and 3.2 wt.%, respectively. The corresponding concentration of Al_2O_3 is 1.9, 4.9 and 3.7 mole% for fibers F1, F2, and F3, respectively.

Preprints (www.preprints.org) | NOT PEER-REVIEWED | Posted: 30 August 2020 doi:10.20944/preprints202008.0666.v1

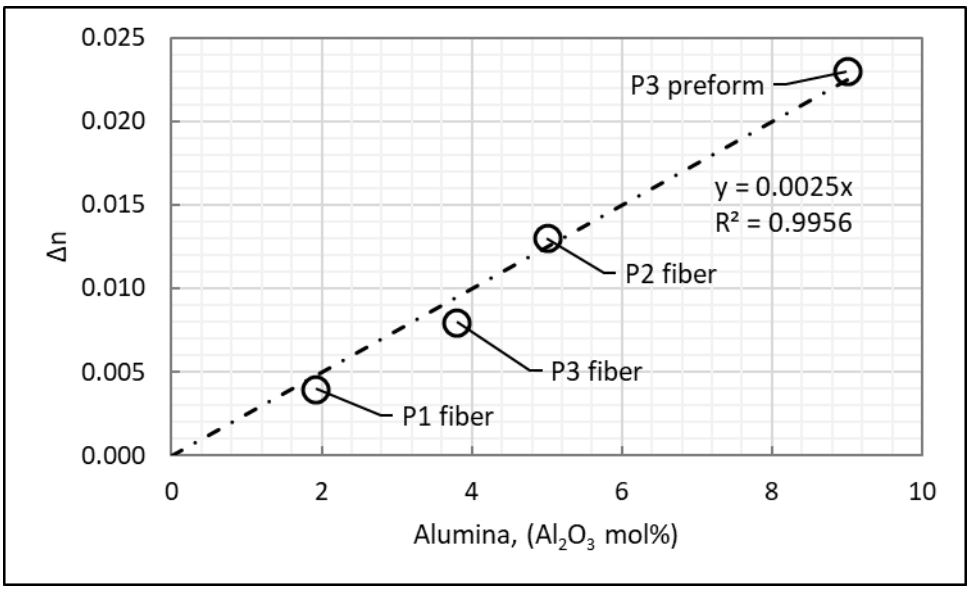

Figure 10. Plot of the refractive index difference vs. mol% of alumina in the range of 0 to 9 mol%. The refractive index of silica increases by 0.0025 per mol% of Al_2O_3.

5. Conclusions

We reported an initial study on alumina doped silica preforms/fibers fabricated by MCVD vapor phase technique using $Al(acac)_3$ as the precursor. The $Al(acac)_3$ sublimation temperature as well as the deposition direction (i.e. downstream and upstream) were varied while keeping other parameters such as oxygen flow rate and deposition temperature fixed. At a sublimation temperature of 185°C, the process efficiency was found to be 21%. For the downstream deposition, the longitudinal uniformity for Δn and core size was observed to be significantly higher than the combined downstream/upstream deposition (%RSD Δn and core size < 2% and < 2.4%, respectively vs. 55% and 18%, respectively). We also reported on the refractive index change per mol% of Al_2O_3 and it was found to be 0.0025. The optical and spectroscopic properties of the fabricated fibers are currently being thoroughly studied by our group.

Author Contributions: Conceptualization, K.S., N.O., and H.R.; methodology and investigation, K.S., N.O., M.Z., and S.Y.; data curation and analysis, K.S., M.Z., and S.Y.; data validation, N.O. and H.R.; writing—original draft preparation, K.S.; writing—review and editing, N.O., M.Z., S.Y., and H.R..; supervision, H.R.; project administration, N.O.; funding acquisition, H.R.

Funding: The authors would like to thank Telekom Malaysia through its R&D subsidiary (TMR&D) for supporting this project.

Conflicts of Interest: The authors declare no conflict of interest.

References

1. Maurer, R.D.; Schultz, P.C. Fused Silica Optical Waveguide. US Patent No. 3659915, **1972**.
2. Simpson, J.R.; Macchesney, J.B. Alternate Dopants for Silicate Wave-Guides. In Proceedings of the Optical Fiber Communication; Optical Society of America, 1982; p. TuCC5. https://doi.org/10.1364/OFC.1982.TuCC5.
3. Ohmori, Y.; Miya, T.; Horiguchi, M. Transmission-Loss Characteristics of Al_2O_3-Doped Silica Fibers. *Journal of Lightwave Technology* **1983**, *1*, 50–56. https://doi.org/10.1109/JLT.1983.1072067.
4. Roba, G. Method of Fabricating Alumina-Doped Silica Fibers. US Patent No. 4657575, **1987**.
5. Wang, J.; Li, M-j.; Nolan, D.A. The Lowest-Loss of 0.35 dB/km in an Aluminum-Doped SM Optical Fiber. In Proceedings of the 2006 Optical Fiber Communication Conference and the National Fiber Optic Engineers Conference; 2006; p. 3 pp. https://doi.org/10.1109/OFC.2006.215677.

6. Wang, J. Alumina as a Dopant in Optical Fiber by OVD. *Applied Physics A* **2014**, *116*, 505–518. https://doi.org/10.1007/s00339-014-8525-x.
7. Čampelj, S.; Perpar, L.; Lukan, P.; Štajner, J.; Ramšak, A.; Lenardič, A.; Lenardič, B. Background Attenuation of Al-Doped Fibers Produced with Vapor Phase Doping Technique. In Proceedings of the Workshop on Specialty Optical Fibers and Their Applications; Optical Society of America, 2015; p. WT4A.8. https://doi.org/10.1364/WSOF.2015.WT4A.8.
8. Muhd-Yassin, S.Z.; Omar, N.Y.M.; Mat-Sharif, K.A.; Zulkifli, M.I.; Safar, M.H.; Aljamimi, S.M.; Yusoff, Z.; Emami, S.D.; Paul, M.C.; Abdul-Rashid, H.A. Solution Doped Preform with Improved Uniformity and Concentration Using Dual-Layer Soot Deposition. *Optical Fiber Technology* **2016**, *28*, 23–27. https://doi.org/10.1016/j.yofte.2016.01.003.
9. Tumminelli, R.P.; McCollum, B.C.; Snitzer, E. Fabrication of High-Concentration Rare-Earth Doped Optical Fibers Using Chelates. *Journal of Lightwave Technology* **1990**, *8*, 1680–1683. https://doi.org/10.1109/50.60565.
10. Lenardic, B.; Guillon, H.; Bonnafous, S.; Kveder, M. Fabrication of Rare-Earth Doped Fibers by Flash Vaporization Method. In Proceedings of the 33rd European Conference and Exhibition of Optical Communication; 2007; pp. 1–2. https://doi.org/10.1049/ic:20070399.
11. Sekiya, E.H.; Barua, P.; Saito, K.; Ikushima, A.J. Fabrication of Yb-Doped Silica Glass through the Modification of MCVD Process. *Journal of Non-Crystalline Solids* **2008**, *354*, 4737–4742. https://doi.org/10.1016/j.jnoncrysol.2008.04.045.
12. Unger, S.; Lindner, F.; Aichele, C.; Leich, M.; Schwuchow, A.; Kobelke, J.; Dellith, J.; Schuster, K.; Bartelt, H. A Highly Efficient Yb-Doped Silica Laser Fiber Prepared by Gas Phase Doping Technology. *Laser Physics* **2014**, *24*, 035103. https://doi.org/10.1088/1054-660x/24/3/035103.
13. Anuar, K.M.S.; Muhd-Yasin, S.Z.; Zulkifli, M.I.; Hanif, S.; Yusoff, A.; Aljamimi, S.M.; Zubair, H.T.; Yusoff, Z.; Abdul-Rashid, H.A.; Tamchek, N. Er_2O_3-Al_2O_3 Doped Silica Preform Prepared by MCVD-Chelate Vapor Phase Delivery Technique. *Advanced Materials Research* **2014**, *896*, 219–24. https://doi.org/10.4028/www.scientific.net/amr.896.219.
14. Mat-Sharif, K.A.; Omar, N.Y.M.; Hanif, S.; Zulkifli, M.I.; Muhamad-Yassin, S.Z.; Yusoff, A.; Zubair, H.T.; Aljamimi, S.M.; Yusoff, Z.; Abdul-Rashid, H.A.; Tamchek, N. Fabrication of Tm_2O_3/Al_2O_3-Silica Preform by Improved MCVD-Chelate Delivery System. In Proceedings of the 2014 IEEE 5th International Conference on Photonics (ICP); 2014; pp. 119–122. https://doi.org/10.1109/ICP.2014.7002329.
15. Saha, M.; Pal, A.; Pal, M.; Guha, C.; Sen, R. An Optimized Vapor Phase Doping Process to Fabricate Large Core Yb-Doped Fibers. *Journal of Lightwave Technology* **2015**, *33*, 3533–3541. https://doi.org/10.1109/JLT.2015.2442226.
16. Mat-Sharif, K.A.; Omar, N.Y.M.; Zulkifli, M.I.; Muhd-Yassin, S.Z.; Sin, Y.K.; Abdul-Rashid, H.A.; Tamchek, N. Highly Tm Doped Silica Optical Preform by MCVD - Chelate Vapor Delivery (Soot-Dopant Stepwise Technique). *Key Engineering Materials* **2018**, *780*, 57–61. https://doi.org/10.4028/www.scientific.net/kem.780.57.
17. Semyannikov, P.P.; Igumenov, I.K.; Trubin, S.V.; Chusova, T.P.; Semenova, Z.I. Thermodynamics of Sublimation of Aluminium Triacetylacetonate. *Thermochimica Acta* **2006**, *451*, 80–83. https://doi.org/10.1016/j.tca.2006.08.008.
18. Walker, K.L.; Geyling, F.T.; Nagel, S.R. Thermophoretic Deposition of Small Particles in the Modified Chemical Vapor Deposition (MCVD) Process. *Journal of the American Ceramic Society* **1980**, *63*, 552–558. https://doi.org/10.1111/j.1151-2916.1980.tb10763.x.
19. Tang, F.Z.; McNamara, P.; Barton, G.W.; Ringer, S.P. Nanoscale Characterization of Silica Soots and Aluminium Solution Doping in Optical Fibre Fabrication. *Journal of Non-Crystalline Solids* **2006**, *352*, 3799–3807. https://doi.org/10.1016/j.jnoncrysol.2006.06.014.
20. Krichhof, J.; Unger, S.; Grau, L.; Funke, A.; Kleinert, P. A New MCVD Technique for Increased Efficiency of Dopant Incorporation in Optical Fibre Fabrication. *Crystal Research and Technology* **1990**, *25*, K29–K34. https://doi.org/10.1002/crat.2170250223.
21. Tang, F.Z.; McNamara, P.; Barton, G.W.; Ringer, S.P. Multiple Solution-Doping in Optical Fibre Fabrication I – Aluminium Doping. *Journal of Non-Crystalline Solids* **2008**, *354*, 927–937. https://doi.org/10.1016/j.jnoncrysol.2007.08.020.

22. Bubnov, M.M.; Gur'yanov, A.N.; Salganskii, M.Yu.; Khopin, V.F. Reaction of Germanium Tetrachloride with Oxygen under MCVD Fiber Preform Fabrication Conditions. *Inorganic Materials* **2007**, *43*, 968–971. https://doi.org/10.1134/S0020168507090105.
23. Abramov, A.N.; Yashkov, M.V.; Guryanov, A.N.; Melkumov, M.A.; Dvoretskii, D.A.; Bufetov, I.A.; Iskhakova, L.D.; Koltashev, V.V.; Kachenyuk, M.N.; Torsunov, M.F. Fabrication and Optical Characterization of Silica Fibers with a Chromium- and Alumina-Doped Core. *Inorganic Materials* **2014**, *50*, 1283–1288. https://doi.org/10.1134/S0020168514110016.
24. Bubnov, M.M.; Gur'yanov, A.N.; Zotov, K.V.; Iskhakova, L.D.; Lavrishchev, S.V.; Lipatov, D.S.; Likhachev, M.E.; Rybaltovsky, A.A.; Khopin, V.F.; Yashkov, M.V.; Dianov, E.M. Optical Properties of Fibres with Aluminophosphosilicate Glass Cores. *Quantum Electronics* **2009**, *39*, 857–862. https://doi.org/10.1070/qe2009v039n09abeh014007.